The Mesoporous Metal–Organic Framework MIL-101 at High Pressure

Anna Celeste, Annalisa Paolone, Jean-Paul Itié, Ferenc Borondics, Boby Joseph, Oana Grad, Gabriela Blanita, Claudia Zlotea, Francesco Capitani

The Mesoporous Metal–Organic Framework MIL-101 at High-Pressure

Anna Celeste[1,2], Annalisa Paolone[3], Jean-Paul Itié[2], Ferenc Borondics[2], Boby Joseph[4], Oana Grad[5], Gabriela Blanita[5], Claudia Zlotea[1], Francesco Capitani[2]*

[1] Institut de Chimie et des Matériaux Paris-Est, CNRS UMR 7182, UPEC, 2-8, rue Henri Dunant, 94320 Thiais, France;

[2] Synchrotron SOLEIL, L'Orme des Merisiers, Saint-Aubin, 91192 Gif sur Yvette Cedex, France;

[3] Consiglio Nazionale delle Ricerche – Istituto dei Sistemi Complessi, U.O.S. La Sapienza, Piazzale A. Moro 5, 00185 Rome, Italy;

[4] Elettra-Sincrotrone Trieste - S.S. 14-km 163.5, 34149 Basovizza, Trieste, Italy;

[5] National Institute for Research and Development of Isotopic and Molecular Technologies, 67-103 Donat Str., RO-400293 Cluj-Napoca, Romania

ABSTRACT: The chromium terephthalate MIL-101 is a mesoporous metal-organic framework (MOF) with unprecedented adsorption capacities due to the presence of giant pores. The application of an external pressure can effectively modify the open structure of MOFs and its interaction with guest molecules. In this work, we study MIL-101 under pressure by synchrotron X-ray diffraction and infrared (IR) spectroscopy with several pressure transmitting media (PTM). Our experimental results clearly show that when a solid medium as NaCl is employed, an irreversible amorphization of the empty structure occurs at about 0.4 GPa. Using a fluid PTM, as Nujol or high-viscosity silicone oil, results in a slight lattice expansion and a strong modification of the peak frequency and shape of the MOF hydroxyl vibration below 0.1 GPa. Moreover, the framework stability is enhanced under pressure with the amorphization onset shifted to about 7 GPa. This coherent set of results points out the insertion of the fluid inside the MIL-101 pores. Above 7 GPa, concomitantly to the nucleation of the amorphous phase, we observe a peculiar medium-dependent lattice expansion. The behavior of the OH stretching vibrations under pressure is profoundly affected by the presence of the guest fluid, showing that OH bonds are sensitive vibrational probes of the host-guest interactions. The present study demonstrates that even a polydimethylsiloxane silicone oil, although highly viscous, can be effectively inserted into the MIL-101 pores at a pressure below 0.2 GPa. High pressure can thus promote the incorporation of large polymers in mesoporous MOFs.

INTRODUCTION

The large number of possible combinations of organic linkers with metallic clusters or ions[1,2] have allowed the synthesis of tens of thousands of porous metal-organic frameworks (MOFs) up to date.[3] This unprecedented chemical versatility makes MOFs suitable for a wide range of applications[4], with a particular focus on gas storage, delivery and separation.[5,6] MOFs, as other porous systems, can be classified by pore size in microporous (pore diameter d < 20 Å), mesoporous (20 Å < d < 50 Å) and macroporous (d > 50 Å). Much attention has been devoted to mesoporous MOFs since, along with the same advantages of the microporous frameworks, their large structural voids allow new physical and chemical functionalities.[7,8] Among these possibilities, probably the most valuable are the adsorption of large molecules, functionalization with complex functional groups[7,8], encapsulation of nanometric objects[9], and separation in the liquid phase, essential for heterogeneous catalysis applications.[10]

The MOF's large surface-to-volume ratio can be effectively tuned by external stimuli, such as pressure, which in turn influence both the structure and adsorption properties of the material. Previous studies carried out on microporous MOFs have shown that compression in the GPa range reveals interesting phenomena, both related to the host framework, such as negative linear compressibility[11–13], reversible pore closing[14–16], amorphization[17–19], and to the guest molecules, such as enhanced sorption properties[20] or small molecules inclusion.[21–27] The investigation of MOFs mechanical response to pressure also showed that they are good candidates as mechanical energy absorbers, thus of interest as deformable materials for shock dissipation.[28,29]

Mechanical stability of MOFs is of paramount importance for industrial applications, where practical processing involves compression, such as extrusion or pelletization, are commonly performed. Therefore, the study of MOFs under pressure has a twofold advantage of providing fundamental insights on the mechanical properties of porous framework and the host-guest interactions which is crucial for industrial processes as well.

To the best of our knowledge, until now, only microporous MOFs have been studied under pressure mainly by X-ray diffraction.[21–23,30] Reports on the structural response of mesoporous MOFs to pressure are currently lacking in the literature.[17] The presence of mesopores allows to explore the possibility of using high pressure as alternative to synthetic methods to incorporate large molecules giving birth

to a composite material with new chemical and physical properties.[31,32]

Here, we report the high-pressure (HP) response of the mesoporous MIL-101 by means of synchrotron X-ray diffraction (XRD) and infrared (IR) spectroscopy in the presence of several pressure transmitting media. MIL-101 (Material Institute Lavoisier) is a chromium terephthalate made of trimeric chromium oxide units combined with terephthalic acid as linker, as shown in Fig. 1. They give rise to a structure of quasi-spherical pores, with diameters about 29 and 34 Å, which translates into a high BET surface area (≈ 3600 m^2 g^{-1}).[33] The large pore size combined with excellent hydrothermal and chemical stability and its high adsorption capacity makes MIL-101 an ideal mesoporous MOF for many applications.[34–36] We demonstrate that the HP behavior of the empty-pore MIL-101 is obtained with a solid pressure transmitting medium (PTM), and it is characterized by a pressure-induced amorphization at about 0.4 GPa. Using a large molecular fluid PTM results in pore filling which enhances the framework stability up to about 7 GPa. We show that the mesoporous nature of MIL-101 and the HP treatment even allows the incorporation of a large polymer as polydimethylsiloxane (PDMS).

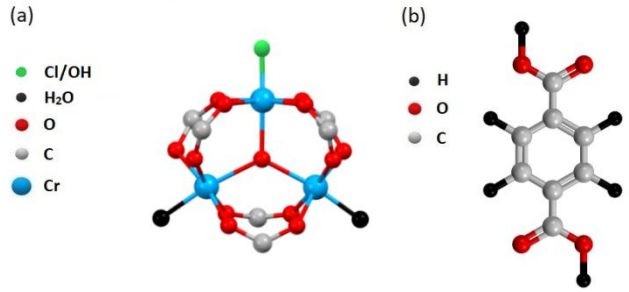

Figure 1. Representation of the chromium oxide trimeric building block (a) and the organic linker, terephthalic acid (b).

EXPERIMENTAL

MIL-101 $(Cr_3O)Cl_x(OH)_{1-x}(H_2O)_2[O_2C\text{-}C_6H_4\text{-}CO_2]_3(H_2O)_n$ was obtained from terephthalic acid, chromium chloride hexahydrate and water, following a green synthetic path (see Supplementary Information for further details on the synthesis protocol). The powder sample was then activated by heating under reflux with ethanol for 24 hours and later dried at 423 K for 10 hours.[36,37] The textural properties of the synthesized MIL-101 were estimated by nitrogen adsorption/desorption isotherm, shown in Fig. S2, resulting in a BET surface area of 3549 m^2 g^{-1} and a specific pore volume of 1.72 cm^3 g^{-1} (see Fig. S3 for the pore size distribution).

Activated samples were stored and manipulated in a glovebox under N_2 gas atmosphere (O_2 and H_2O levels < 1 ppm) and never exposed to air. In addition to this controlled storage condition, samples were degassed under vacuum (below 10^{-5} mbar) at 493 K for 18 h before every experiment. This procedure ensured the removal of guest molecules possibly adsorbed over the storage periods inside the glovebox.

MIL-101 was first characterized at ambient conditions by high-resolution synchrotron X-ray powder diffraction at the XRD1 beamline of the ELETTRA synchrotron (Italy). The sample was loaded inside a capillary in a glovebox. Diffraction images were collected using a DECTRIS Pilatus 2M detector with an X-ray beam wavelength of 0.7 Å. At ELETTRA we also performed some preliminary HP XRD measurements at the Xpress beamline (see Fig. S4).

High-pressure XRD and IR measurements were performed at the SOLEIL synchrotron (France) on the PSICHE and SMIS beamlines, respectively. Membrane diamond anvil cells (DACs) equipped with diamonds of different culet sizes (400-1000 µm) were used, depending on the pressure range explored. Type IIas diamonds were used in the IR range. 125 – 300 µm diameter holes were drilled in stainless steel or copper gaskets pre-indented to around 50 µm thickness. Sample loading was performed inside a glovebox equipped with a microscope. The DAC was sealed to a pressure value around 0.1 GPa before removing it from the glovebox. Four PTM were used: two fluids, PDMS silicone oil (viscosity 30000 cSt at 25°C, CAS Number 63148-62-9) and the mineral oil Nujol (viscosity 100 cSt at 25°C, CAS nr. 8012-95-1),and solid salts, namely NaCl for XRD and CsI for IR.[38] The solid PTM were finely milled, dried and stored at 120 °C in an oven before loading in the DAC. Pressure was determined in situ by the ruby fluorescence technique for IR measurements[39], while it was obtained through the equation of state of NaCl for XRD measurements (a few grains of NaCl were inserted in the cell even when using fluid PTM).[40] Fluid PTM can be considered hydrostatic up to around 12 GPa while alkali halides ensure a pressure standard deviation below 0.1 GPa in the pressure range explored here.[38,41,42]

HP XRD data were collected at the PSICHE beamline with a 0.48975 Å X-ray beam focused by Kirkpatrick-Baez mirrors on a 35 $µm^2$ spot and using a DECTRIS CdTe 4M detector. 2D diffraction images were converted to 1D patterns using the Dioptas software.[43] The Le Bail refinement method was used to extract unit cell parameters at each pressure. IR spectroscopy measurements were performed at the SMIS beamline, where a home-built horizontal microscope equipped with large working distance Schwarzschild objectives allows HP measurements from the near to the far infrared (FIR) domain. The microscope is coupled with a Thermo-Fisher iS50 Fourier Transform IR interferometer and uses the synchrotron radiation as the light source. FIR spectra were collected with a liquid He cooled Si bolometer in the 200-700 cm^{-1} spectral range while an N_2 cooled MCT/A detector was used in the mid infrared range (MIR) between 700-4000 cm^{-1}.

In order to compare IR and XRD measurements and to avoid different kinetics of transformation, pressure was increased for both experiments at a rate of about 0.05 - 0.1 GPa per minute on average. The pressure equilibration time was about 5 minutes for each point. IR spectra and XRD pattern collection time was around 2 minutes.

RESULTS AND DISCUSSION

The XRD pattern of MIL-101 powder under a 1 bar Ar atmosphere in a capillary is shown in Fig. S5, together with

the Le Bail refinement obtained with the Fd$\bar{3}$m cubic structure reported in the literature. The obtained unit cell parameters are listed in Table 1 and are consistent with the previous ones of 88.87 Å and 701860 Å^3 initially reported by Férey *et al*.[33] This measurement sets our ambient pressure structural model to be compared with the following HP measurements.

Selected HP XRD patterns of MIL-101 are shown in Fig. 2 in the low 2θ region, with NaCl (a), silicone oil (b) and Nujol (c) used as PTM (the full 2θ range is shown in Fig. S6). With NaCl as PTM, the intensity of the Bragg peaks gradually decreases under pressure up to about 0.4 GPa, where the XRD pattern of MIL-101 is no longer detectable (see Fig. 2(a)). This indicates a complete transition to an amorphous phase which is not reversible after the pressure release (as further confirmed when MIL-101 is compressed without PTM, see Fig. S7).

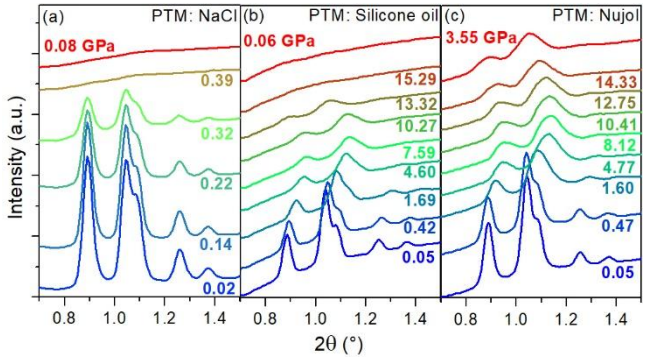

Figure 2. Selected powder XRD patterns (λ = 0.48975 Å) of MIL-101 under pressure with (a) NaCl, (b) silicone oil and (c) Nujol as PTM. Patterns are vertically stacked for sake of clarity with increasing pressure values in GPa. Patterns collected after the pressure release, at the lowest possible pressure, are shown in red.

XRD patterns with fluid PTM, silicone oil and Nujol, present a common behavior as a function of pressure (see Fig. 2(b)-(c)). Increasing pressure, Bragg reflections shift toward higher angles up to about 7 GPa, indicating the lattice compression. Above this pressure, surprisingly, peaks shift towards lower angles while simultaneously becoming broader and less intense.

Above about 13 GPa, MIL-101 shows different structural responses depending on the fluid PTM. With silicone oil, the XRD signal completely disappears, indicating that the sample becomes completely amorphous. This latter phase is maintained when the pressure is released to 0.1 GPa (see Fig. 2(b)). When Nujol is used, the main XRD peaks are still present at 14.3 GPa although very broad, indicating that long-range order is partly preserved. Decreasing pressure to 3.5 GPa does not re-establish the original crystallinity, with the XRD pattern shape resembling that collected at the highest pressure (see Fig. 2(c)).

The enhanced framework stability under pressure with fluid PTM strongly suggests the penetration of the PTM into the MIL-101 pores,[17–19,25] which is not possible with the solid NaCl. Indeed, the inclusion of Nujol, made of long-chain alkanes, was expected since the average molecular size is smaller than MIL-101 pore windows (12-16 Å).[25,44] We observed a similar behavior when using silicone oil and Nujol as PTM, which suggests that even silicone oil, made of long PDMS chains, can enter into the pores despite its high viscosity.

To verify this hypothesis, we performed a Le Bail refinement at each pressure value using the cubic Fd$\bar{3}$m structure assuming that this is maintained before the crystal-to-amorphous transition. The lattice parameters and volumes obtained for the lowest pressure points with the three PTM are compared in Table l to those obtained at ambient pressure in a capillary. This comparison shows that the cubic lattice parameter *a* of MIL-101 in the capillary and in the DAC with NaCl are compatible. On the contrary, when fluid PTM are used, *a* results to be larger than the lattice parameter obtained with the pristine MIL-101 in the capillary. In particular, *a* increases of 0.64 Å with silicone oil and of 0.39 Å with Nujol. This indicates that the insertion of fluid PTM already starts when the DAC is initially closed, at a pressure lower than 0.1 GPa, resulting in a slightly expanded lattice.

Table 1. Unit cell parameters of MIL-101 obtained through the Le Bail refinement for sample inside the capillary and inside the DAC with different PTM at the lowest pressure.

PTM	P (GPa)	*a* (Å)	$V/10^2$ (Å^3)
None (capillary)	0	88.31±0.03	6893.8±1.0
NaCl	0.02	88.25±0.03	6872.6±3.9
Silicone Oil	0.05	88.95±0.03	7037.5±7.6
Nujol	0.05	88.70±0.03	6977.6±6.2

The relative change in the lattice parameter *a* under pressure is shown in Fig. 3(a) up to 0.8 GPa, for the three PTM. In the presence of NaCl, *a* is nearly constant while increasing pressure, until the amorphization process is completed at about 0.4 GPa. This behavior reflects the lack of a pressure-induced shift of the Bragg peaks, as visible in Fig. 2a, and can be explained by the concomitant formation of the amorphous phase starting at 0.1 GPa, as witnessed by the peak intensity reduction. In other words, pressure causes a strong compression of a sample portion which becomes amorphous already at the lowest pressure measured, while the rest of the sample remains crystalline and gives the diffraction signal up to 0.4 GPa, without experiencing a detectable lattice compression. Note that the lattice constant possibly increases between 0.2 GPa and 0.4 GPa. Despite a few pressure points and a larger uncertainty due to the amorphization, this expansion could be real, as it will be discussed more in detail in the case of fluid PTM.

When MIL-101 is loaded with Nujol, *a* decreases almost linearly, reaching a -1.5% relative change at 0.7 GPa. With silicone oil, interestingly, the lattice parameter relative change exhibits two different regions of almost linear compressibility, below and above 0.2 GPa, as shown in detail in Fig. S8. First, it decreases with a slope of -0.01 GPa^{-1} and then of -0.03 GPa^{-1}, thus showing a threefold increase above 0.2 GPa. This behavior is reminiscent to that observed for the Cu-btc framework under pressure, with a fluid PTM of small molecules, such as methanol-ethanol mixture and isopropyl alcohol.[22] In analogy with that study, MIL-101 is less compressible in the low-pressure regime since the PTM penetrates into the cavities until they are hyperfilled at a certain pressure threshold (about

0.2 GPa with silicone oil). After this value, the framework and PTM are compressed together. This also explains why MIL-101 with Nujol does not show the two-regime behavior. The framework is already hyperfilled when the DAC is loaded at pressures lower than 0.1 GPa, because alkanes in Nujol have a smaller size.

The pressure dependence of the lattice parameter *a* thus confirms the insertion of Nujol and silicone oil inside the pores of MIL-101 at HP, in agreement with both the slight lattice expansion observed upon DAC closing and the pressure-induced amorphization shifted to higher pressure when fluids are used.

In Figure 3(b), *a* is shown as a function of pressure up to 15 GPa, for the two fluid PTM. Above 0.8 GPa, the lattice parameter decreases in a similar way with both PTM, up to about 7 GPa. At higher pressure, it unexpectedly starts to increase with pressure. This effect is more pronounced for silicone oil than Nujol, indicating a possible link with the molecular size of the PTM. At these pressures the MIL-101 structure is quite disordered, as can be seen in Fig. 2 and S5, with low-intensity and high-angle Bragg reflections (above about 3°) not detectable anymore while the main peaks become quite broad. As discussed before in the NaCl case, this points to the nucleation of an amorphous phase coexisting with a crystalline one (which gives the diffraction signal). These two phases and the PTM represent a closed thermodynamic system, whose total volume has to decrease under pressure. Therefore, the observed lattice expansion of the crystalline phase is allowed if a strong volume reduction of another component takes place at the same time. We hypothesize the amorphous phase has a higher density because its pores are collapsed, as it has been already observed in other MOFs.[45,46] This creates the space necessary for the expansion of the crystalline phase. The migration of the guest molecules from the collapsed pores of the amorphous into the crystal could also contribute to the expansion, explaining the larger increase of the parameter *a* observed with silicone oil, as shown in Fig. 3(b). This phenomenon, although complex, has been recently proposed to explain a similar pressure-induced expansion in microporous systems.[47,48]

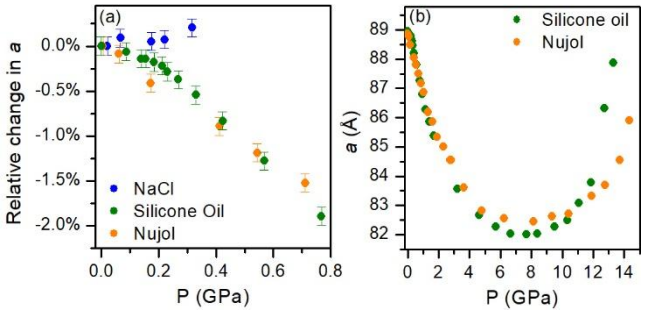

Figure 3. (a) Relative change in the unit cell parameter *a* of MIL-101 under pressure up to 0.8 GPa. (b) Pressure dependence of the lattice parameter *a*. NaCl (blue symbol), silicone oil (green) and Nujol (orange) are the PTM employed. Error bars are within the symbol size.

In order to further confirm the observed structural transformations, the PTM inclusion and to obtain local and chemical information, we performed HP synchrotron-based IR measurements. IR spectra of MIL-101 as loaded inside the DAC at 0.1 GPa are shown in Fig. 4 in the 200 – 3800 cm^{-1} spectral range, for three PTM. Generally in MOFs, collective vibrational modes and metallic cluster vibrations are active in the FIR region (typically below 600 cm^{-1}), while absorption peaks in the MIR range are due to internal vibrations of the organic linker.[49–51] An unambiguous assignment of the MIL-101 IR modes is still missing in the literature. However, the comparison with other terephthalate or chromium oxide based MOFs, such as MIL-53,[52,53] MIL-68,[25] UiO-66[54] and MIL-100[55,56] allows an identification of the main spectral features. We base the vibrational assignment on the spectrum collected with CsI as PTM (see Fig. 4(a)), since with a solid PTM the MIL-101 structure is empty.

Starting from the FIR range shown in Fig. 4 (b), the peak at 389 cm^{-1} has been not reported before and it is assigned *a posteriori* to a collective mode, based on its response to pressure. The peak at 589 cm^{-1} is attributed to a CrO vibration. The bands between 700 and 1200 cm^{-1} are assigned to the bending of benzene rings, and the most intense bands between 1300 and 1700 cm^{-1} to the stretching modes of the carboxylate groups. The spectral range within 1800-2400 cm^{-1} is not accessible due to the strong diamond absorption, but typically it does not have any fundamental IR active vibrations.[33] The broad band in the 2700-3600 cm^{-1} region originates from OH stretching vibrations of residual water molecules inside the pores and from the MOF hydroxyl groups perturbed by the hydrogen bonding with water.[54] On the high-frequency side of this band, shown in Fig. 4(c), two peaks emerge, a weak one at 3590 cm^{-1} (labeled ν_1) and another one more intense at 3669 cm^{-1} (ν_2). Based on previous works on MIL-100,[56] these two modes can be assigned to the OH stretching of the isolated Cr-OH and Cr-H_2O groups, respectively. It is important to stress that the measurements of the OH peaks, which will provide valuable insights in the following, have been possible thanks to the careful sample preparation. In fact, proper sample degassing before each measurement and DAC loading inside the glovebox are crucial to observe the two OH peaks, otherwise covered by a strong and broad water band appearing in a few minutes after air exposure (see Fig. S12).

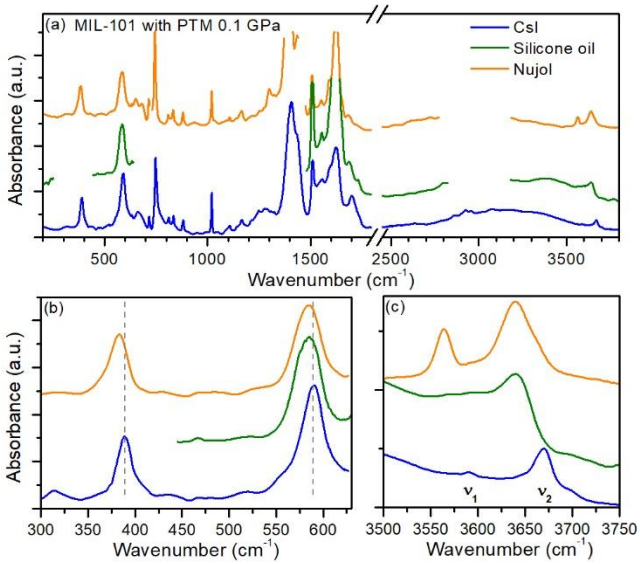

Figure 4. (a) IR spectra of MIL-101 loaded in the DAC with CsI (blue), Nujol (orange) and silicone oil (green) at 0.1 GPa. Spectral regions where signal saturates due to silicone oil or Nujol absorptions are masked. (b) FIR region where the collective mode and the CrO vibration appear. Grey dashed lines represents the peak central frequency with CsI and highlight the frequency shift with fluid PTM. (c) Spectral region of the OH stretching vibrations. Spectra are vertically stacked for clarity.

The comparison between the spectrum collected with CsI and the two with Nujol and silicone oil points out some spectral modifications induced by the fluid PTM (silicone oil and Nujol IR spectra shown in Fig. S13). Besides a new peak appearing with Nujol around 1300 cm^{-1}, the main differences are found in the FIR (Fig. 4(b)) and in the OH stretching region (Fig. 4(c)). The collective mode at 389 cm^{-1}, the CrO mode at 589 cm^{-1} and the ν_1-ν_2 OH modes all appear broader and shifted to lower frequencies by the presence of fluid PTM (see Fig. S14). In particular, the collective mode frequency measured with Nujol shows the strongest softening relative to its frequency with CsI, about -1.5%, whereas the other three modes are shifted of about -0.8 %, as shown in Fig. S14. The softening of the collective mode is explained by the fluid-induced lattice expansion observed by XRD (see Table I). The softening of OH vibrations can be interpreted as the effect of steric interactions between the incorporated molecules and the Cr-OH/H_2O groups inside the pores. This, in turn, also affects the CrO vibrational frequency. These results create a coherent vibrational picture consistent with the PTM insertion within the MOF pores and indicate that the aforementioned modes are ideal vibrational probes of the host-guest interaction. We will now focus on their behavior at high-pressure.

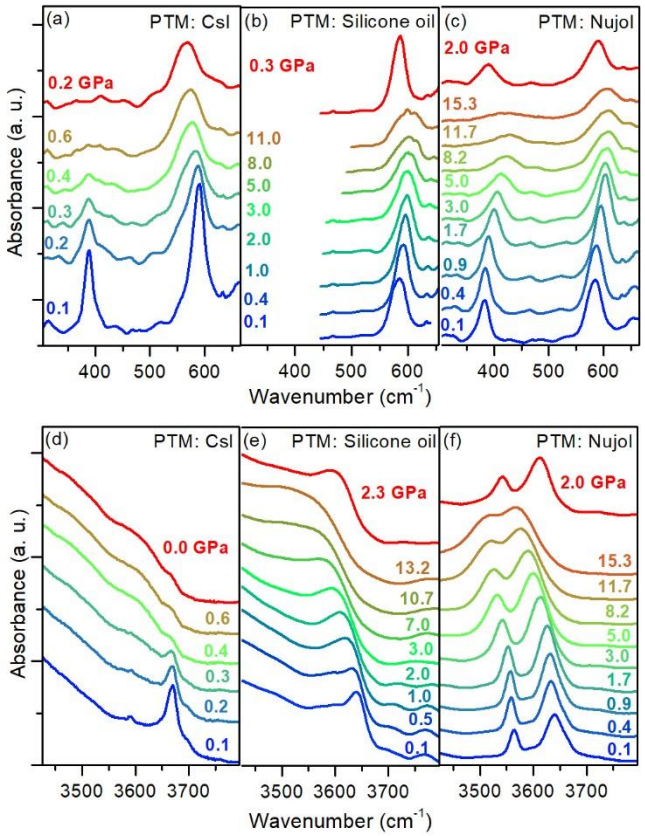

Figure 5. Selected FIR and OH stretching regions of MIL-101 spectra measured under pressure with CsI (a)-(d), silicone oil (b)-(e) and Nujol (c)-(f) used as PTM. In panel (b), the absorption around 400 cm^{-1} of silicone oil is masked. Spectra collected after the pressure release, at the lowest possible pressure, are shown in red. Spectra are vertically stacked for clarity with increasing pressure values.

HP IR spectra of MIL-101 measured with three PTM in the two relevant spectral ranges, FIR and in OH stretching region, are shown in Fig. 5, whereas the whole frequency range is shown in Fig. S15. When CsI is used (panels (a)-(d)), the collective mode around 389 cm^{-1} and the intensity of the two OH modes ν_1 and ν_2 become weaker as pressure increases without a significant frequency shift, until they completely disappear at about 0.4 GPa. The CrO peak at 589 cm^{-1} shows a clear softening and broadening up to 0.4 GPa, while little effect is observed at higher pressures. The pressure-induced spectral changes are not reversible after the release of pressure. This behavior is consistent with the irreversible crystalline-to-amorphous transition occurring at 0.4 GPa, as observed in the XRD measurements (see Fig. 2(a)), and it confirms that the peak at 389 cm^{-1} is a collective mode, not present when the long-range order is lost. The collapse of the pores also leads to an increased interaction of the terminal OH bonds with the surrounding environment, witnessed by the ν_1 and ν_2 peaks fading into the broad band below 3700 cm^{-1}.

With fluid PTM, a common behavior is observed both in the FIR and OH regions (Fig. 5 (b)-(e) for silicone oil, (c)-(f) for Nujol). The collective mode around 389 cm^{-1} is not detectable with silicone oil due to the strong PTM absorption, but it can be measured with Nujol. In this case it hardens and broadens with pressure but it is present over the whole pressure range. The CrO vibration, accessible both with Nujol and silicone oil, has a similar evolution under pressure. In the OH stretching region both ν_1 and ν_2 show a remarkable and unexpected pressure-induced softening, along with a line-shape broadening.

Therefore with fluid PTM, both FIR and OH modes have an opposite behavior than with CsI. Peak broadening under pressure indicates the increasing disorder although a complete amorphization is not reached in the IR experiments with fluid media. In fact, releasing the pressure, all the observed spectral changes are partly reversible both in peak shapes and positions. The presence of the collective mode up to 15.3 GPa with Nujol and the lack of new peaks appearing, demonstrate the enhanced framework stability at HP with a fluid PTM. This is in well agreement with XRD results, which showed that MIL-101 cubic structure is still present at 11 / 13.2 GPa with silicone oil and at 15.3 GPa with Nujol. The continuous and apparent softening of the two OH modes indicates that the PTM-MOF interaction are effectively and continuously tuned by pressure, with the steric interactions becoming stronger when PTM and Cr-OH /Cr-H_2O groups get closer under pressure.

Finally, it is worth noting that the CrO and the ligand vibrational peaks, shown in Fig. 5(a)-(c) and S15 respectively, are still detected at the highest pressures reached with all the PTM. Therefore the MIL-101 building units, *i.e.* chromium cluster and terephthalic acid, are stressed by the

pressure treatment but still preserved even when the MIL-101 becomes completely amorphous.

CONCLUSIONS

In this work we have investigated, for the first time to our knowledge, the effect of high-pressure on the mesoporous MOF MIL-101 using different (fluid and solid) pressure transmitting media. The combination of two complementary synchrotron techniques and a thorough sample preparation allowed us to obtain a clear and consistent picture about the effect of external pressure on MIL-101. High-pressure behavior of empty-pore MIL-101 is obtained only when a solid PTM is used. Indeed, with NaCl a crystal-to-amorphous transitions starts already at 0.1 GPa and it is completed at about 0.4 GPa, where the whole XRD pattern, a collective IR mode and the OH stretching bands disappear, representing experimental markers to determine whether sample preparations and applications involving a compression transform MIL-101 into an amorphous.

Using a fluid PTM as Nujol or high-viscosity PDMS silicone oil, the framework stability increases up to 7 GPa, due to PTM penetration inside the pores. Above this pressure, a peculiar pressure-induced expansion of the crystalline phase is observed which is explained by the concomitant nucleation of a denser amorphous phase. The size of this expansion is dependent on the fluid PTM. The amorphization process is complete around 15 GPa with silicone oil, whereas with Nujol it is still not completed at about 14 GPa. The insertion of the fluid PTM is further confirmed by IR spectroscopy, where the OH stretching vibrations of the MOF hydroxyl groups and their pressure dependence are strongly modified by the presence of the guest PTM inside the pores. In particular, we demonstrate that high-pressure allows the incorporation of high-viscosity PDMS silicone oil inside the large pores of MIL-101, proving that hybridization of MOFs with polymers can be achieved by industrially accessible pressure treatments, in addition with widely reported chemical synthetic methods. This could be of interest for very large-molecules segregation, separation and other technological applications made possible by mesoporous MOFs.

ASSOCIATED CONTENT

Supporting Information.

Synthesis methods, N_2 adsorption and desorption measurements, pore size distribution, preliminary XRD, Le Bail fit of the capillary XRD, full 2θ range of the high-pressure XRD measurements with and without PTM, bulk moduli and Birch-Murnaghan fit, IR spectrum of air-exposed MIL-101, IR spectra of oils, full frequency range of the MIR spectra at high-pressure.

AUTHOR INFORMATION

Corresponding Author

* francesco.capitani@synchrotron-soleil.fr

Notes

The authors declare no competing financial interest.

ACKNOWLEDGMENT

A.C, C.Z. and G.B. acknowledge the French National Research Agency (ANR) and the Romanian Ministry of Education and Research (UEFISCDI) for the financial support under MEMOS contract ANR-15-CE05-0012-01 and PN-II-ID-JRP-RO-FR-2015-0025, respectively. The authors gratefully acknowledge synchrotron SOLEIL (proposals #20190370 and #20190878) and ELETTRA (#20185235 and #20190313) for provision of beamtime. A.C, A.P. and F.C. acknowledge the project CALIPSOplus (Grant Agreement 730872) from the EU Framework Programme for Research and Innovation HORIZON2020 for financial support for beamtimes at synchrotrons SOLEIL and ELETTRA.
Maurizio Polentarutti and Giorgio Bais are acknowledged for support at XRD1 while Alain Polian and Abdelmalek Malouche for the help in the experimental preparation. We also wish to thank Oriele Palumbo and Francesco Trequattrini for technical help in the early stage of this research.

REFERENCES

(1) Yaghi, O. M.; O'Keeffe, M.; Ockwig, N. W.; Chae, H. K.; Eddaoudi, M.; Kim, J. Reticular Synthesis and the Design of New Materials. *Nature* **2003**, *423* (6941), 705–714. https://doi.org/10.1038/nature01650.

(2) Maurin, G.; Serre, C.; Cooper, A.; Férey, G. The New Age of MOFs and of Their Porous-Related Solids. *Chem. Soc. Rev.* **2017**, *46* (11), 3104–3107. https://doi.org/10.1039/C7CS90049J.

(3) Chung, Y. G.; Haldoupis, E.; Bucior, B. J.; Haranczyk, M.; Lee, S.; Zhang, H.; Vogiatzis, K. D.; Milisavljevic, M.; Ling, S.; Camp, J. S.; Slater, B.; Siepmann, J. I.; Sholl, D. S.; Snurr, R. Q. Advances, Updates, and Analytics for the Computation-Ready, Experimental Metal–Organic Framework Database: CoRE MOF 2019. *J. Chem. Eng. Data* **2019**, *64* (12), 5985–5998. https://doi.org/10.1021/acs.jced.9b00835.

(4) Furukawa, H.; Cordova, K. E.; O'Keeffe, M.; Yaghi, O. M. The Chemistry and Applications of Metal-Organic Frameworks. *Science* **2013**, *341* (6149). https://doi.org/10.1126/science.1230444.

(5) Li, H.; Wang, K.; Sun, Y.; Lollar, C. T.; Li, J.; Zhou, H.-C. Recent Advances in Gas Storage and Separation Using Metal–Organic Frameworks. *Materials Today* **2018**, *21* (2), 108–121. https://doi.org/10.1016/j.mattod.2017.07.006.

(6) Sumida, K.; Rogow, D. L.; Mason, J. A.; McDonald, T. M.; Bloch, E. D.; Herm, Z. R.; Bae, T.-H.; Long, J. R. Carbon Dioxide Capture in Metal–Organic Frameworks. *Chem. Rev.* **2012**, *112* (2), 724–781. https://doi.org/10.1021/cr2003272.

(7) Xuan, W.; Zhu, C.; Liu, Y.; Cui, Y. Mesoporous Metal–Organic Framework Materials. *Chem. Soc. Rev.* **2012**, *41* (5), 1677–1695. https://doi.org/10.1039/C1CS15196G.

(8) Liu, D.; Zou, D.; Zhu, H.; Zhang, J. Mesoporous Metal–Organic Frameworks: Synthetic Strategies and Emerging Applications. *Small* **2018**, *14* (37), 1801454. https://doi.org/10.1002/smll.201801454.

(9) Yu, J.; Mu, C.; Yan, B.; Qin, X.; Shen, C.; Xue, H.; Pang, H. Nanoparticle/MOF Composites: Preparations and Applications. *Mater. Horiz.* **2017**, *4* (4), 557–569. https://doi.org/10.1039/C6MH00586A.

(10) Senkovska, I.; Kaskel, S. Ultrahigh Porosity in Mesoporous MOFs: Promises and Limitations. *Chem. Commun.* **2014**, *50* (54), 7089–7098. https://doi.org/10.1039/C4CC00524D.

(11) Ortiz, A. U.; Boutin, A.; Gagnon, K. J.; Clearfield, A.; Coudert, F.-X. Remarkable Pressure Responses of Metal–Organic Frameworks: Proton Transfer and Linker Coiling in Zinc Alkyl Gates. *J. Am. Chem. Soc.* **2014**, *136* (32), 11540–11545. https://doi.org/10.1021/ja5060059.

(12) Serra-Crespo, P.; Dikhtiarenko, A.; Stavitski, E.; Juan-Alcañiz, J.; Kapteijn, F.; Coudert, F.-X.; Gascon, J. Experimental Evidence of Negative Linear Compressibility in the MIL-53 Metal–Organic Framework Family. *CrystEngComm* **2014**, *17* (2), 276–280. https://doi.org/10.1039/C4CE00436A.

(13) Li, W.; Probert, M. R.; Kosa, M.; Bennett, T. D.; Thirumurugan, A.; Burwood, R. P.; Parinello, M.; Howard, J. A. K.; Cheetham, A. K. Negative Linear Compressibility of a Metal–Organic Framework. *J. Am. Chem. Soc.* **2012**, *134* (29), 11940–11943. https://doi.org/10.1021/ja305196u.

(14) Serra-Crespo, P.; Stavitski, E.; Kapteijn, F.; Gascon, J. High Compressibility of a Flexible Metal–Organic Framework. *RSC Adv.* **2012**, *2* (12), 5051–5053. https://doi.org/10.1039/C2RA20528A.

(15) Yot, P. G.; Ma, Q.; Haines, J.; Yang, Q.; Ghoufi, A.; Devic, T.; Serre, C.; Dmitriev, V.; Férey, G.; Zhong, C.; Maurin, G. Large Breathing of the MOF MIL-47(VIV) under Mechanical Pressure: A Joint Experimental–Modelling Exploration. *Chem. Sci.* **2012**, *3* (4), 1100–1104. https://doi.org/10.1039/C2SC00745B.

(16) Henke, S.; Wharmby, M. T.; Kieslich, G.; Hante, I.; Schneemann, A.; Wu, Y.; Daisenberger, D.; Cheetham, A. K. Pore Closure in Zeolitic Imidazolate Frameworks under Mechanical Pressure. *Chem. Sci.* **2018**, *9* (6), 1654–1660. https://doi.org/10.1039/C7SC04952H.

(17) Redfern, L. R.; Farha, O. K. Mechanical Properties of Metal–Organic Frameworks. *Chem. Sci.* **2019**, *10* (46), 10666–10679. https://doi.org/10.1039/C9SC04249K.

(18) Collings, I. E.; Goodwin, A. L. Metal–Organic Frameworks under Pressure. *Journal of Applied Physics* **2019**, *126* (18), 181101. https://doi.org/10.1063/1.5126911.

(19) McKellar, S. C.; Moggach, S. A. Structural Studies of Metal–Organic Frameworks under High Pressure. *Acta Cryst B* **2015**, *71* (6), 587–607. https://doi.org/10.1107/S2052520615018168.

(20) Hu, Y.; Liu, Z.; Xu, J.; Huang, Y.; Song, Y. Evidence of Pressure Enhanced CO2 Storage in ZIF-8 Probed by FTIR Spectroscopy. *J. Am. Chem. Soc.* **2013**, *135* (25), 9287–9290. https://doi.org/10.1021/ja403635b.

(21) McKellar, S. C.; Sotelo, J.; Greenaway, A.; Mowat, J. P. S.; Kvam, O.; Morrison, C. A.; Wright, P. A.; Moggach, S. A. Pore Shape Modification of a Microporous Metal–Organic Framework Using High Pressure: Accessing a New Phase with Oversized Guest Molecules. *Chem. Mater.* **2016**, *28* (2), 466–473. https://doi.org/10.1021/acs.chemmater.5b02891.

(22) Chapman, K. W.; Halder, G. J.; Chupas, P. J. Guest-Dependent High Pressure Phenomena in a Nanoporous Metal–Organic Framework Material. *J. Am. Chem. Soc.* **2008**, *130* (32), 10524–10526. https://doi.org/10.1021/ja804079z.

(23) Graham, A. J.; Banu, A.-M.; Düren, T.; Greenaway, A.; McKellar, S. C.; Mowat, J. P. S.; Ward, K.; Wright, P. A.; Moggach, S. A. Stabilization of Scandium Terephthalate MOFs against Reversible Amorphization and Structural Phase Transition by Guest Uptake at Extreme Pressure. *J. Am. Chem. Soc.* **2014**, *136* (24), 8606–8613. https://doi.org/10.1021/ja411934f.

(24) Graham, A. J.; Allan, D. R.; Muszkiewicz, A.; Morrison, C. A.; Moggach, S. A. The Effect of High Pressure on MOF-5: Guest-Induced Modification of Pore Size and Content at High Pressure. *ANGEWANDTE CHEMIE-INTERNATIONAL EDITION* **2011**, *50* (47), 11138–11141. https://doi.org/10.1002/anie.201104285.

(25) Hu, Y.; Lin, B.; He, P.; Li, Y.; Huang, Y.; Song, Y. Probing the Structural Stability of and Enhanced CO2 Storage in MOF MIL-68(In) under High Pressures by FTIR Spectroscopy. *Chemistry – A European Journal* **2015**, *21* (51), 18739–18748. https://doi.org/10.1002/chem.201502980.

(26) Moggach, S. A.; Bennett, T. D.; Cheetham, A. K. The Effect of Pressure on ZIF-8: Increasing Pore Size with Pressure and the Formation of a High-Pressure Phase at 1.47 GPa. *Angew. Chem. Int. Ed. Engl.* **2009**, *48* (38), 7087–7089. https://doi.org/10.1002/anie.200902643.

(27) Kapustin, E. A.; Lee, S.; Alshammari, A. S.; Yaghi, O. M. Molecular Retrofitting Adapts a Metal-Organic Framework to Extreme Pressure. *ACS Cent Sci* **2017**, *3* (6), 662–667. https://doi.org/10.1021/acscentsci.7b00169.

(28) Miao, Y.-R.; Su, Z.; Suslick, K. S. Energy Storage during Compression of Metal–Organic Frameworks. *J. Am. Chem. Soc.* **2017**, *139* (13), 4667–4670. https://doi.org/10.1021/jacs.7b01593.

(29) Yot, P. G.; Vanduyfhuys, L.; Alvarez, E.; Rodriguez, J.; Itié, J.-P.; Fabry, P.; Guillou, N.; Devic, T.; Beurroies, I.; Llewellyn, P. L.; Speybroeck, V. V.; Serre, C.; Maurin, G. Mechanical Energy Storage Performance of an Aluminum Fumarate Metal–Organic Framework. *Chem. Sci.* **2015**, *7* (1), 446–450. https://doi.org/10.1039/C5SC02794B.

(30) Redfern, L. R.; Robison, L.; Wasson, M. C.; Goswami, S.; Lyu, J.; Islamoglu, T.; Chapman, K. W.; Farha, O. K. Porosity Dependence of Compression and Lattice Rigidity in Metal–Organic Framework Series. *J. Am. Chem. Soc.* **2019**, *141* (10), 4365–4371. https://doi.org/10.1021/jacs.8b13009.

(31) Kitao, T.; Zhang, Y.; Kitagawa, S.; Wang, B.; Uemura, T. Hybridization of MOFs and Polymers. *Chem. Soc. Rev.* **2017**, *46* (11), 3108–3133. https://doi.org/10.1039/C7CS00041C.

(32) Lykourinou, V.; Chen, Y.; Wang, X.-S.; Meng, L.; Hoang, T.; Ming, L.-J.; Musselman, R. L.; Ma, S. Immobilization of MP-11 into a Mesoporous Metal–Organic Framework, MP-11@mesoMOF: A New Platform for Enzymatic Catalysis. *J. Am. Chem. Soc.* **2011**, *133* (27), 10382–10385. https://doi.org/10.1021/ja2038003.

(33) Férey, G.; Mellot-Draznieks, C.; Serre, C.; Millange, F.; Dutour, J.; Surblé, S.; Margiolaki, I. A Chromium Terephthalate-Based Solid with Unusually Large Pore Volumes and Surface Area. *Science* **2005**, *309* (5743), 2040–2042. https://doi.org/10.1126/science.1116275.

(34) Llewellyn, P. L.; Bourrelly, S.; Serre, C.; Vimont, A.; Daturi, M.; Hamon, L.; De Weireld, G.; Chang, J.-S.;

Hong, D.-Y.; Kyu Hwang, Y.; Hwa Jhung, S.; Férey, G. High Uptakes of CO2 and CH4 in Mesoporous Metal—Organic Frameworks MIL-100 and MIL-101. *Langmuir* **2008**, *24* (14), 7245–7250. https://doi.org/10.1021/la800227x.

(35) Hong, D.-Y.; Hwang, Y. K.; Serre, C.; Férey, G.; Chang, J.-S. Porous Chromium Terephthalate MIL-101 with Coordinatively Unsaturated Sites: Surface Functionalization, Encapsulation, Sorption and Catalysis. *Advanced Functional Materials* **2009**, *19* (10), 1537–1552. https://doi.org/10.1002/adfm.200801130.

(36) Malouche, A.; Blanita, G.; Lupu, D.; Bourgon, J.; Nelayah, J.; Zlotea, C. Hydrogen Absorption in 1 Nm Pd Clusters Confined in MIL-101(Cr). *J. Mater. Chem. A* **2017**, *5* (44), 23043–23052. https://doi.org/10.1039/C7TA07159K.

(37) Blanita, G.; Lupu, D.; Grad, O.; Misan, I.; Coldea, I.; Borodi, G. Synthetic Method of MIL-101(Cr) Metal-Organic Framework. A01027, December 5, 2017.

(38) Celeste, A.; Borondics, F.; Capitani, F. Hydrostaticity of Pressure-Transmitting Media for High Pressure Infrared Spectroscopy. *High Pressure Research* **2019**, *39* (4), 608–618. https://doi.org/10.1080/08957959.2019.1666844.

(39) Piermarini, G. J.; Block, S.; Barnett, J. D.; Forman, R. A. Calibration of the Pressure Dependence of the R1 Ruby Fluorescence Line to 195 Kbar. *Journal of Applied Physics* **1975**, *46* (6), 2774–2780. https://doi.org/10.1063/1.321957.

(40) Dorogokupets, P. I.; Dewaele, A. Equations of State of MgO, Au, Pt, NaCl-B1, and NaCl-B2: Internally Consistent High-Temperature Pressure Scales. *High Pressure Research* **2007**, *27* (4), 431–446. https://doi.org/10.1080/08957950701659700.

(41) Ragan, D. D.; Clarke, D. R.; Schiferl, D. Silicone Fluid as a High-pressure Medium in Diamond Anvil Cells. *Review of Scientific Instruments* **1996**, *67* (2), 494–496. https://doi.org/10.1063/1.1146627.

(42) Klotz, S.; Chervin, J.-C.; Munsch, P.; Marchand, G. L. Hydrostatic Limits of 11 Pressure Transmitting Media. *J. Phys. D: Appl. Phys.* **2009**, *42* (7), 075413. https://doi.org/10.1088/0022-3727/42/7/075413.

(43) Prescher, C.; Prakapenka, V. B. DIOPTAS: A Program for Reduction of Two-Dimensional X-Ray Diffraction Data and Data Exploration. *High Pressure Research* **2015**, *35* (3), 223–230. https://doi.org/10.1080/08957959.2015.1059835.

(44) Grice, K.; Mesmay, R. de; Glucina, A.; Wang, S. An Improved and Rapid 5A Molecular Sieve Method for Gas Chromatography Isotope Ratio Mass Spectrometry of N-Alkanes (C8–C30+). *Organic Geochemistry* **2008**, *39* (3), 284–288. https://doi.org/10.1016/j.orggeochem.2007.12.009.

(45) Hu, Y. H.; Zhang, L. Amorphization of Metal-Organic Framework MOF-5 at Unusually Low Applied Pressure. *Phys. Rev. B* **2010**, *81* (17), 174103. https://doi.org/10.1103/PhysRevB.81.174103.

(46) Su, Z.; Miao, Y.-R.; Mao, S.-M.; Zhang, G.-H.; Dillon, S.; Miller, J. T.; Suslick, K. S. Compression-Induced Deformation of Individual Metal–Organic Framework Microcrystals. *J. Am. Chem. Soc.* **2015**, *137* (5), 1750–1753. https://doi.org/10.1021/ja5113436.

(47) Sobczak, S.; Katrusiak, A. Zone-Collapse Amorphization Mimicking the Negative Compressibility of a Porous Compound. *Crystal Growth & Design* **2018**, *18* (2), 1082–1089. https://doi.org/10.1021/acs.cgd.7b01535.

(48) Li, Q.; Li, S.; Wang, K.; Liu, J.; Yang, K.; Liu, B.; Zou, G.; Zou, B. High-Pressure Studies of Abnormal Guest-Dependent Expansion in {[Cu(CO3)2](CH6N3)2}n. *J. Phys. Chem. C* **2014**, *118* (11), 5848–5853. https://doi.org/10.1021/jp412105a.

(49) Bonino, F.; Lamberti, C.; Bordiga, S. IR and Raman Spectroscopies Probing MOFs Structure, Defectivity, and Reactivity; 2016. https://doi.org/10.1002/9783527693078.ch22.

(50) Ryder, M. R.; Civalleri, B.; Bennett, T. D.; Henke, S.; Rudić, S.; Cinque, G.; Fernandez-Alonso, F.; Tan, J.-C. Identifying the Role of Terahertz Vibrations in Metal-Organic Frameworks: From Gate-Opening Phenomenon to Shear-Driven Structural Destabilization. *Phys. Rev. Lett.* **2014**, *113* (21), 215502. https://doi.org/10.1103/PhysRevLett.113.215502.

(51) Ryder, M. R.; Civalleri, B.; Cinque, G.; Tan, J.-C. Discovering Connections between Terahertz Vibrations and Elasticity Underpinning the Collective Dynamics of the HKUST-1 Metal–Organic Framework. *CrystEngComm* **2016**, *18* (23), 4303–4312. https://doi.org/10.1039/C5CE02347E.

(52) Hoffman, A. E. J.; Vanduyfhuys, L.; Nevjestić, I.; Wieme, J.; Rogge, S. M. J.; Depauw, H.; Van Der Voort, P.; Vrielinck, H.; Van Speybroeck, V. Elucidating the Vibrational Fingerprint of the Flexible Metal-Organic Framework MIL-53(Al) Using a Combined Experimental/Computational Approach. *J Phys Chem C Nanomater Interfaces* **2018**, *122* (5), 2734–2746. https://doi.org/10.1021/acs.jpcc.7b11031.

(53) Volkringer, C.; Loiseau, T.; Guillou, N.; Férey, G.; Elkaïm, E.; Vimont, A. XRD and IR Structural Investigations of a Particular Breathing Effect in the MOF-Type Gallium Terephthalate MIL-53(Ga). *Dalton Trans.* **2009**, No. 12, 2241–2249. https://doi.org/10.1039/B817563B.

(54) Shearer, G. C.; Forselv, S.; Chavan, S.; Bordiga, S.; Mathisen, K.; Bjørgen, M.; Svelle, S.; Lillerud, K. P. In Situ Infrared Spectroscopic and Gravimetric Characterisation of the Solvent Removal and Dehydroxylation of the Metal Organic Frameworks UiO-66 and UiO-67. *Top Catal* **2013**, *56* (9), 770–782. https://doi.org/10.1007/s11244-013-0027-0.

(55) Vimont, A.; Goupil, J.-M.; Lavalley, J.-C.; Daturi, M.; Surblé, S.; Serre, C.; Millange, F.; Férey, G.; Audebrand, N. Investigation of Acid Sites in a Zeotypic Giant Pores Chromium(III) Carboxylate. *J. Am. Chem. Soc.* **2006**, *128* (10), 3218–3227. https://doi.org/10.1021/ja056906s.

(56) Volkringer, C.; Leclerc, H.; Lavalley, J.-C.; Loiseau, T.; Férey, G.; Daturi, M.; Vimont, A. Infrared Spectroscopy Investigation of the Acid Sites in the Metal–Organic Framework Aluminum Trimesate MIL-100(Al). *J. Phys. Chem. C* **2012**, *116* (9), 5710–5719. https://doi.org/10.1021/jp210671t.

Authors are required to submit a graphic entry for the Table of Contents (TOC) that, in conjunction with the manuscript title, should give the reader a representative idea of one of the following: A key structure, reaction, equation, concept, or theorem, etc., that is discussed in the manuscript. Consult the journal's Instructions for Authors for TOC graphic specifications.

Insert Table of Contents artwork here